Electronic Supplementary Material (ESI) for RSC Advances.

Synthesis and characterisation of permethylindenyl zirconium complexes and their use in ethylene polymerisation

Jean-Charles Buffet, Thomas A. Q. Arnold, Zoë R. Turner, Phakpoom Angpanitcharoen, and Dermot O'Hare*

Chemistry Research Laboratory, 12 Mansfield Road, OX1 3TA, Oxford, UK.

E-mail: dermot.ohare@chem.ox.ac.uk.

Table of contents

1. Experimental details

General details. Air and moisture sensitive compounds were manipulated under an inert atmosphere of nitrogen, using standard Schlenk line techniques on a dual manifold vacuum/nitrogen line or a Braun Unilab glove box. Reaction solvents (pentane, hexane, toluene, DCM) were dried using an MBraun SPS 800 solvent purification system. Diethylether and thf were distilled from purple Na/benzophenone indicator. Toluene and hexane were stored over potassium-mirrored ampoules. Pentane, diethylether and thf were stored over pre-activated 3 Å molecular sieves. Dry solvents were stored in oven-dried ampoules under an atmosphere of nitrogen, sealed with either Rotaflo or Young's taps. Deuterated solvents used in NMR spectroscopic analysis of air-sensitive compounds were dried over NaK (benzene-d_6) and CaH (chloroform-d_1), freeze-thaw degassed, vacuum transferred and stored over pre-activated 3 Å molecular sieves. benzene-d_6 and chloroform-d_1 were purchased from Goss Scientific. *rac*-(EBI)$ZrCl_2$ (Strem Chemicals) was purchased and used as received. Methylaluminoxane (Sigma-Aldrich) was purchased as a toluene solution and dried *in vacuo* to afford a white, crystalline solid before use.

Solution phase nuclear magnetic resonance spectroscopy Air sensitive samples were prepared under an inert atmosphere in a glove box, using dried solvents in Young's taps NMR tubes. ^{1}H NMR spectra were recorded at 298 K unless stated otherwise on Bruker AVIII 400 nanobay or 300 MHz Varian Mercury VxWorks spectrometers. ^{1}H (300.27 MHz) and $^{13}C\{^{1}H\}$ (75.50 MHz) and $^{13}C\{1H\}$ s[ectra on the same spectrometers at 75 and 100 MHz respectively. NMR spectra were referenced internally to the residual protio-solvent resonances in the deuterated solvent used. ^{1}H and $^{13}C\{^{1}H\}$ chemical shifts, δ, are given in parts per million (ppm) relative to tetramethylsilane ($\delta = 0$).

Solid State Nuclear Magnetic Resonance Spectroscopy Solid state NMR spectra were recorded by Dr. Nicholas H. Rees (University of Oxford) on a Varian Chemagnetics CMX Infinity 200 (4.7 T) spectrometer operating at 50.3, 52.1 and 39.8 MHz for ^{13}C, ^{27}Al and ^{29}Si respectively. Samples were packed in 7.5 mm zirconia rotors. A double resonance MAS probe was used for all measurements and MAS rate of 4 kHz was used for ^{13}C and ^{29}Si, whereas MAS rate of 6 kHz was used for ^{27}Al. ^{13}C CPMAS NMR spectra were acquired with a cross-polarisation sequence with a variable X-amplitude spin-lock pulse and phase modulated proton decoupling was used. 13,000 transients were acquired using a contact time of 1 ms, an acquisition time of 41 ms (1024 data points zero filled to 16 K) and a recycle delay of 30 s. All ^{13}C spectra were referenced to adamantane (the upfield methine resonance was taken to be at $\delta = 29.5$ ppm on a scale where $\delta(TMS) = 0$) as a secondary reference. ^{27}Al MAS NMR spectra were acquired with a single pulse excitation was applied using a short pulse length (0.7 μs). Each spectrum resulted from 2000 scans separated by a 1 s delay. The ^{27}Al chemical shifts are referenced to an aqueous solution of $Al(NO_3)_3$ ($\delta = 0$ ppm). In order to obtain quantitative ^{29}Si DPMAS NMR spectra, typical 5000 transients were acquired with an acquisition time of 68 ms (1024 data points zero filled to 16 K) and a recycle delay of 30 s. All ^{29}Si spectra were externally referenced to kaolinite (taken to be at $\delta = -91.7$ ppm on a scale where $\delta(TMS) = 0$) as a secondary reference.

Scanning Electron Microscopy Scanning electron microscopy (SEM) analysis was performed with the help of Jennifer Holter on a JEOL JSM 6610LV scanning electron microscope with an accelerating voltage of 3.0 kV. Samples were spread on carbon tape adhered to an SEM stage. Before imaging, the samples were coated with a thin platinum layer to prevent charging and to improve the image quality.

Gel Permeation Chromatography Gel permeation chromatography (GPC) data were collected by Supote Sibtute on a high temperature gel permeation chromatograph with a IR5 infrared detector (GPC-IR5). Samples were prepared by dissolution in 1,2,4-trichlorobenzene (TCB) containing 300 ppm of 3,5-di-*tert*-butyl-4-hydroxytoluene (BHT) at 160 °C for 90 minutes and then filtered with a 10 μm SS filter before being passed through the GPC column. The samples were run under a flow rate of 0.5 ml/min using TCB containing 300 ppm of BHT as mobile phase with 1 mg/ml BHT added as a flow rate marker. The GPC column and detector temperature were set at 145 °C and 160 °C respectively.

X-ray crystallography. Crystals were mounted on MiTeGen Micromounts with a perfluoropolyether oil (Fomblin YR1800, Alfa Aesar) and cooled rapidly to 150 K using an Oxford Cryosystems Cryostream unit.[1] Two different diffractometer setups were used as follows: 1) An Enraf-Nonius Kappa CCD diffractometer using graphite monochromated Mo Kα radiation (λ = 0.71073 Å). Raw frame data were reduced using the DENZO-SMN package,[2] and corrected for absorption using SORTAV.[3] Intensity data were collected using a multi-scan method with SCALEPACK (within DENZO-SMN) and 2) An Oxford Diffraction Supernova using multilayer, orthogonal, micro-focus Cu Kα radiation (λ = 1.5405 Å). Raw frame data were collected, reduced and processed using CrysAlisPro.[4] The structures were solved using either direct methods with SHELXS,[5] or using charge-flipping with SuperFlip,[6] and refined using a full-matrix least squares refinement on all F^2 data using the CRYSTALS[7,8] or Win-GX[9] program suite. In general, distances were calculated using the full variance/co-variance matrix. Dihedral angles were calculated with CCDC's Mercury[10] or using PLATON.[11] Illustrations of the solid-state molecular structures were created using ORTEP.[12]

Density functional theory calculations.

All DFT calculations were performed with the ORCA program package.[13] The geometry optimizations of the complexes and single-point calculations on the optimized geometries were carried out at the BP86[14-16] or B3LYP[14, 17, 18] level of DFT. The def2-TZVP(-f) basis set in the scalar relativistic recontraction reported by Neese *et al.* (segmented all-electron relativistic basis sets, SARC) was applied.[19, 20] For all elements up to bromine, the SARC basis sets are simply scalar relativistic recontractions of the basis sets developed by the Karlsruhe group,[21, 22] while for heavier elements, the primitives and contraction patterns were designed in references 19 and 20. The Coulomb fitting basis set of Weigend[23] was used in uncontracted form in all calculations. The RI[24-26] approximation was used to accelerate the calculations. Orbitals were generated with the program Chimera, with the isosurface limits at ± 0.05.[27]

Mass spectrometry. Samples were run as electron impact (EI) mass spectra and the data were collected by Mr. Colin Sparrow (University of Oxford).

Elemental analysis. Samples were prepared in the glovebox and sealed in glass tubes (i.d. 2.5 mm, o.d. 5 mm) under vacuum. CHN analyses were carried out by Dr. Stephen Boyer, London Metropolitan University in duplicate.

Gel permeation chromatography. GPC characterisations were carried out by Dr. P. Thipphaya at SCG Chemicals, Ltd (Thailand) in Rayong on high temperature GPC-IR from Polymer Char using a IR5 MCT detector. The GPC samples were dissolved at 140 °C in dichlorobenzene and shake for 18 h. The samples recovery was targeted over 95%.

2. X-ray crystallography

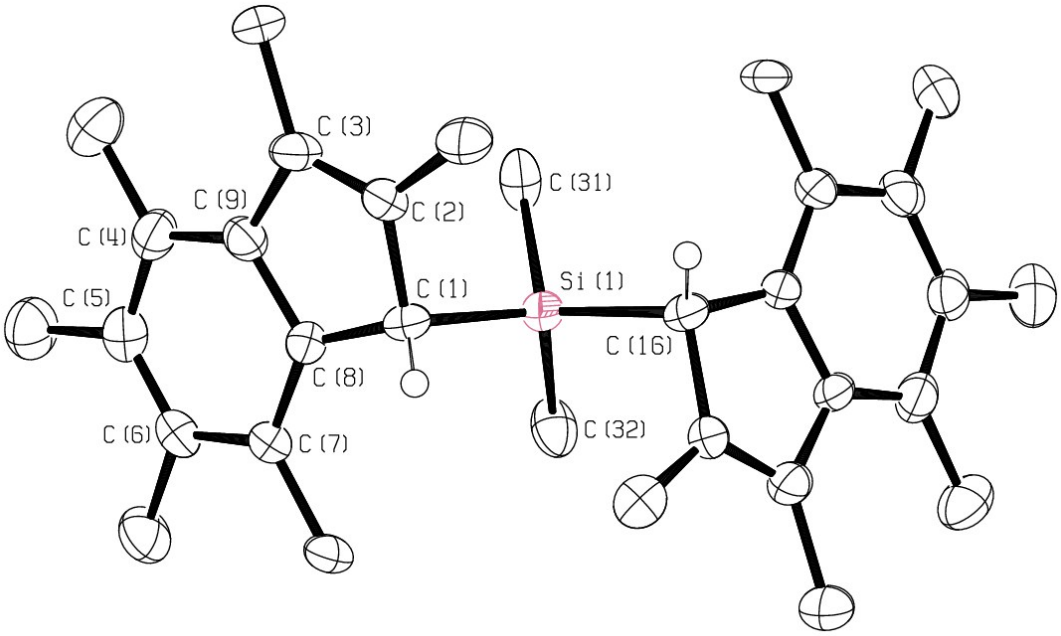

Fig. S1: Solid-state molecular structure of (*S,S*)-*rac*-(SBI*)H_2. H atoms, apart from those on C(1) and C(16) omitted for clarity. Thermal ellipsoids drawn at 50%.

Table S1: Selected bond lengths and angles for *rac*-(SBI*)H_2.

Bond Lengths (Å)			
C(1)-C(2)	1.502(5)	C(17)-C(18)	1.500(6)
C(2)-C(3)	1.347(6)	C(18)-C(19)	1.341(6)
C(3)-C(9)	1.477(6)	C(19)-C(25)	1.492(6)
C(8)-C(9)	1.410(5)	C(24)-C(25)	1.410(6)
C(1)-C(8)	1.510(6)	C(17)-C(24)	1.498(5)
C(4)-C(9)	1.406(6)	C(20)-C(25)	1.404(6)
C(4)-C(5)	1.407(6)	C(20)-C(21)	1.406(7)
C(5)-C(6)	1.416(6)	C(21)-C(22)	1.391(7)
C(6)-C(7)	1.399(6)	C(22)-C(23)	1.413(6)
C(7)-C(8)	1.395(6)	C(23)-C(24)	1.400(6)
C(1)-Si(1)	1.937(4)	C(16)-Si(1)	1.941(4)
Bond Angles (°)			
C(1)-Si(1)-C(16)	110.69(18)	C(31)-Si(1)-C(33)	106.3(2)

Table S2. Crystallography parameters for *rac*-(SBI*)H_2

Chemical formula	$C_{32}H_{44}Si$
M_r	456.79
Crystal system, space group	Triclinic, $P\bar{1}$
Temperature (K)	150
a, b, c (Å)	9.2291 (7), 9.7804 (7), 15.8873 (12)
β (°)	89.600 (6), 81.392 (6), 73.234 (6)
V (Å^3)	1356.64 (18)
Z	2
Radiation type	Cu Kα
μ (mm^{-1})	0.87
Crystal size (mm)	0.15 × 0.05 × 0.03
Data collection	
Diffractometer	Oxford Diffraction SuperNova diffractometer
Absorption correction	Multi-scan CrysAlisPro
T_{min}, T_{max}	0.52, 0.97
No. of measured, independent and observed [$I > 2.0\sigma(I)$] reflections	5617, 5617, 4511
R_{int}	0.081
$(\sin \theta/\lambda)_{max}$ (Å^{-1})	0.631
Refinement	
$R[F^2 > 2\sigma(F^2)]$, $wR(F^2)$, S	0.097, 0.279, 0.97
No. of reflections	5595
No. of parameters	301
H-atom treatment	H-atom parameters constrained
$\Delta\rho_{max}$, $\Delta\rho_{min}$ (e Å^{-3})	0.57, −0.39

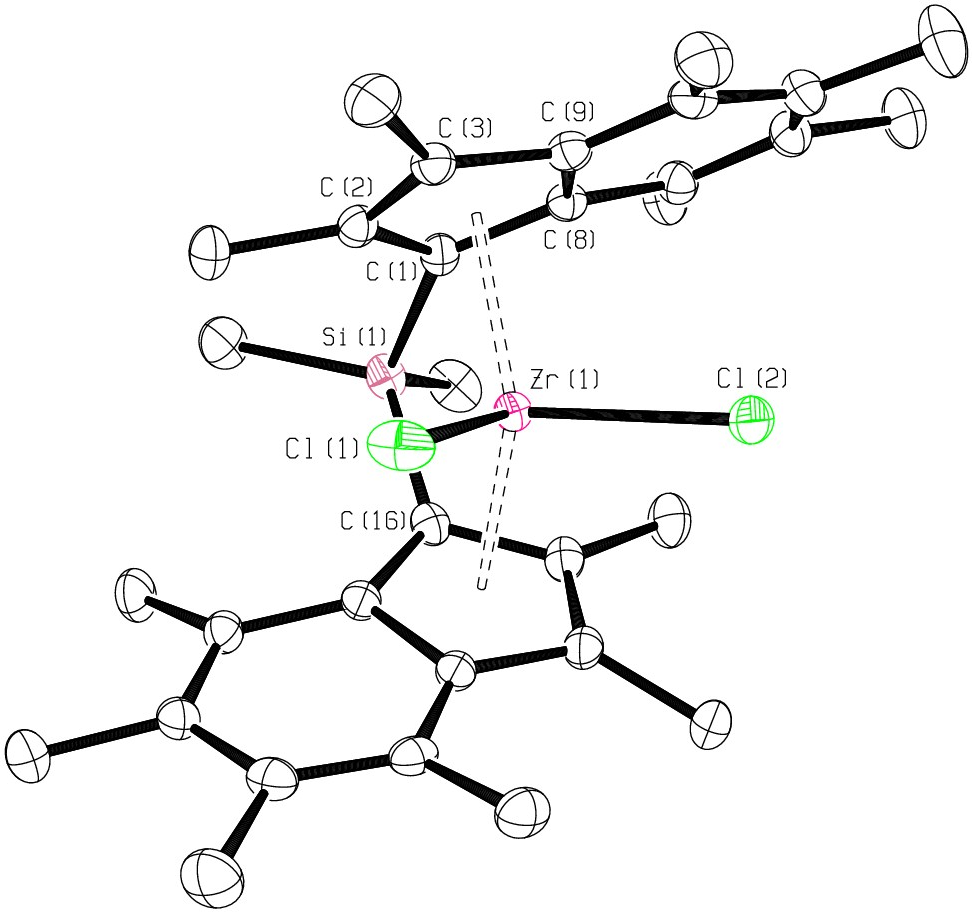

Fig. S2 Molecular structure of *rac*-(SBI*)$ZrCl_2$. H atoms omitted for clarity. Thermal ellipsoids drawn at 50%.

Table S3: Selected bond lengths (Å), angles (°), and geometric parameters (Å/°) for *rac*-(SBI*)$ZrCl_2$. Estimated standard deviations .

Bond Lengths			
Zr(1)-Cp_{cent}	2.257	Zr(1)-Cp_{cent}	2.244
Zr(1)-C(1)	2.4628 (16)	Zr(1)-C(16)	2.4740 (16)
Zr(1)-C(2)	2.4807 (17)	Zr(1)-C(17)	2.4697 (17)
Zr(1)-C(3)	2.5952 (17)	Zr(1)-C(18)	2.5992 (17)
Zr(1)-C(8)	2.6012 (17)	Zr(1)-C(23)	2.6439 (17)
Zr(1)-C(9)	2.6339 (17)	Zr(1)-C(24)	2.6428 (17)
Zr(1)-Cl(1)	2.4195 (5)	Zr(1)-Cl(2)	2.4255 (4)
C(1)-Si(1)	1.8986 (18)	C(16)-Si(1)	1.8979 (18)
Si(1)-C(31)	1.875 (2)	Si(1)-C(32)	1.872 (2)
Avg. Cp C-C	1.439	Avg. Cp C-C	1.439
Avg. Cp C-Me	1.506	Avg. Cp C-Me	1.506
Avg. C_6 C-C	1.418	Avg. C_6 C-C	1.419
Avg. C_6 C-Me	1.511	Avg. C_6 C-Me	1.509
Δ_{M-C}	0.105	Δ_{M-C}	0.129
Bond Angles			
C(1)-Si(1)-C(16)	96.22(7)	C(31)-Si(1)-C(32)	98.70(10)
Cl(1)-Zr(1)-Cl(2)	97.797(19)		
α	58.50	δ	130.35
β	18.49	β	18.89
TA′	145.15	RA	116.89
HA	5.01	HA	4.13
FA	9.80	FA	5.81

Table S4. Crystallographic data for *rac*-(SBI*)$ZrCl_2$

Chemical formula	$C_{32}H_{42}Cl_2SiZr$
M_r	616.90
Crystal system, space group	Monoclinic, $P2_1/n$
Temperature (K)	150
a, b, c (Å)	14.1078 (1), 14.2840 (2), 14.3753 (2)
β (°)	96.8940 (5)
V (Å^3)	2875.91 (6)
Z	4
Radiation type	Mo Kα
μ (mm^{-1})	0.63
Crystal size (mm)	0.35 × 0.30 × 0.25
Data collection	
Diffractometer	Nonius KappaCCD diffractometer
Absorption correction	Multi-scan *DENZO*/*SCALEPACK*
T_{min}, T_{max}	0.77, 0.85
No. of measured, independent and observed [$I > 2.0\sigma(I)$] reflections	12519, 6559, 5817
R_{int}	0.013
$(\sin\theta/\lambda)_{max}$ (Å^{-1})	0.649
Refinement	
$R[F^2 > 2\sigma(F^2)]$, $wR(F^2)$, S	0.030, 0.076, 1.10
No. of reflections	6559
No. of parameters	339
H-atom treatment	H-atom parameters constrained
$\Delta\rho_{max}$, $\Delta\rho_{min}$ (e Å^{-3})	0.56, −0.53

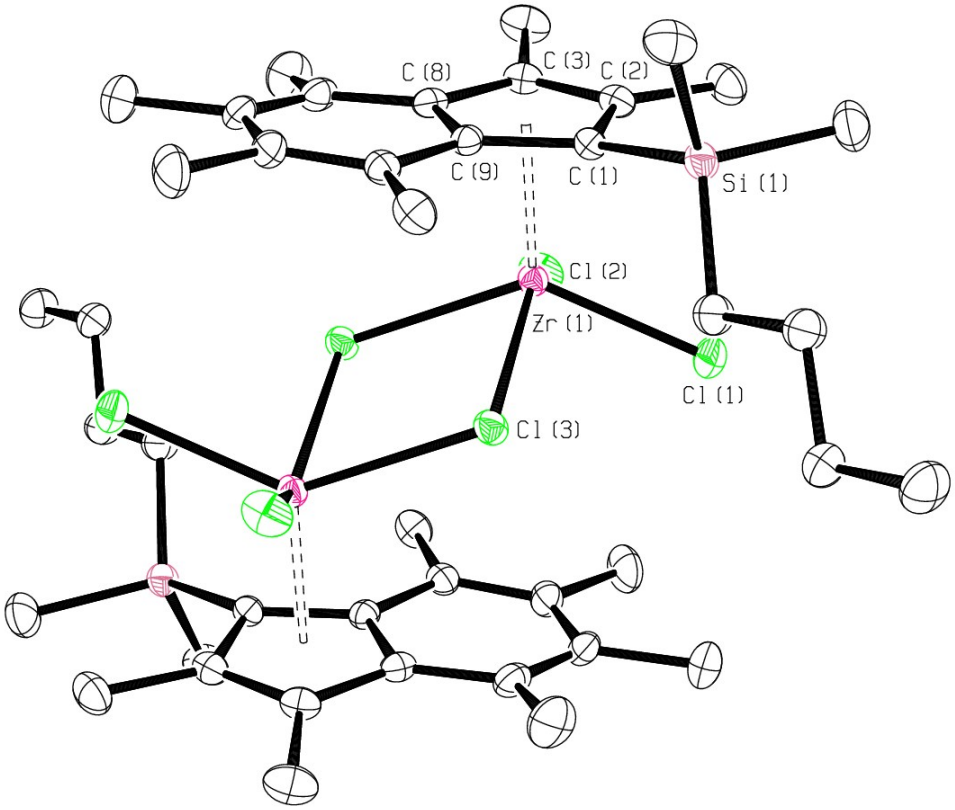

Fig. S3 Solid-state molecular structure of $[(Ind^*SiMe_2{}^nBu)Zr(\mu\text{-}Cl)Cl_2]_2$. H atoms omitted for clarity. Thermal ellipsoids drawn at 50%.

Table S5: Selected bond lengths (Å), angles (°), and geometric parameters (Å/°) for $[(Ind^*SiMe_2{}^nBu)Zr(\mu\text{-}Cl)Cl_2]_2$.

Bond Lengths			
Zr(1)-Cp_{cent}	2.190	Zr(1)-C(3)	2.5623 (16)
Zr(1)-C(1)	2.4294 (16)	Zr(1)-C(8)	2.5201 (16)
Zr(1)-C(2)	2.4645 (16)	Zr(1)-C(9)	2.5673 (16)
Zr(1)-Cl(1)	2.3982 (4)	Zr(1)-Cl(2)	2.4037 (4)
Zr(1)-Cl(3)	2.5837 (4)	Zr(1)-Cl(3)′	2.5837 (4)
Si(1)-C(1)	1.9128 (17)		
Avg. Cp C-C	1.442	Avg. C_6 C-C	1.418
Avg. Cp C-Me	1.508	Avg. C_6 C-Me	1.513
$\Delta_{M\text{-}C}$	0.058		
Bond Angles			
Cl(1)-Zr(1)-Cl(2)	91.233 (17)	Cl(1)-Zr(1)-Cl(3)	82.776 (15)
Cl(2)-Zr(1)-Cl(3)	137.879 (15)	Cl(3)-Zr(1)-Cl(3)′	74.715 (14)
FA	3.71		

Table S6. Crystallography parameters for $[(Ind^*SiMe_2{}^nBu)Zr(\mu\text{-}Cl)Cl_2]_2$

Chemical formula	$C_{21}H_{33}Cl_3SiZr$
M_r	511.16
Crystal system, space group	Triclinic, $P\bar{1}$
Temperature (K)	150
a, b, c (Å)	9.5271 (1), 11.1274 (1), 11.3616 (1)
β (°)	78.1654 (5), 87.3403 (5), 77.9022 (5)
V (Å^3)	1152.67 (2)
Z	2
Radiation type	Mo *K*a
μ (mm^{-1})	0.88
Crystal size (mm)	0.36 × 0.32 × 0.22
Data collection	
Diffractometer	Nonius KappaCCD diffractometer
Absorption correction	Multi-scan *DENZO*/*SCALEPACK*
T_{min}, T_{max}	0.72, 0.82
No. of measured, independent and observed [$I > 2.0\sigma(I)$] reflections	34494, 5248, 4881
R_{int}	0.013
$(\sin\theta/\lambda)_{max}$ (Å^{-1})	0.649
Refinement	
$R[F^2 > 2\sigma(F^2)]$, $wR(F^2)$, S	0.027, 0.070, 0.93
No. of reflections	5248
No. of parameters	244
H-atom treatment	H-atom parameters constrained
$\Delta\rho_{max}$, $\Delta\rho_{min}$ (e Å^{-3})	0.50, −0.62

3. NMR Spectroscopy

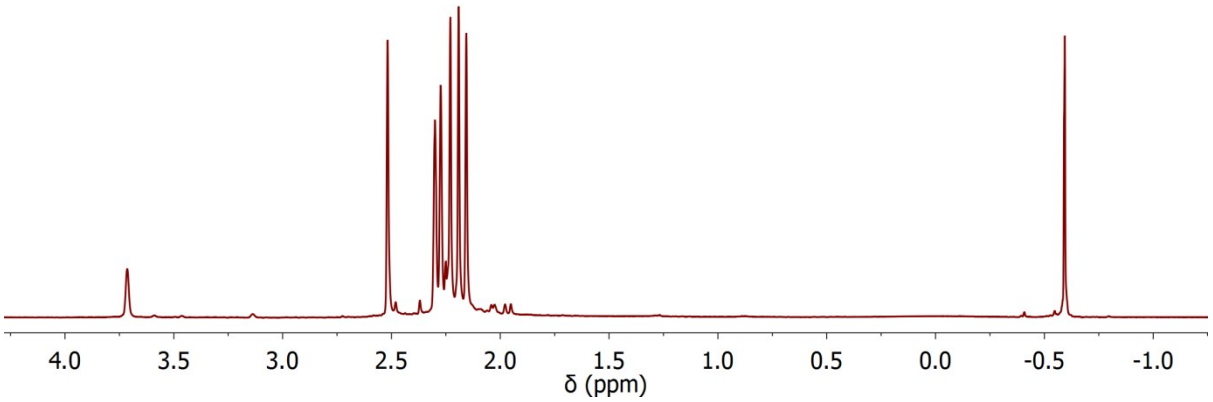

Fig. S4: ^{1}H NMR spectrum of *rac*-(SBI*)H_2 in chloroform-d_1.

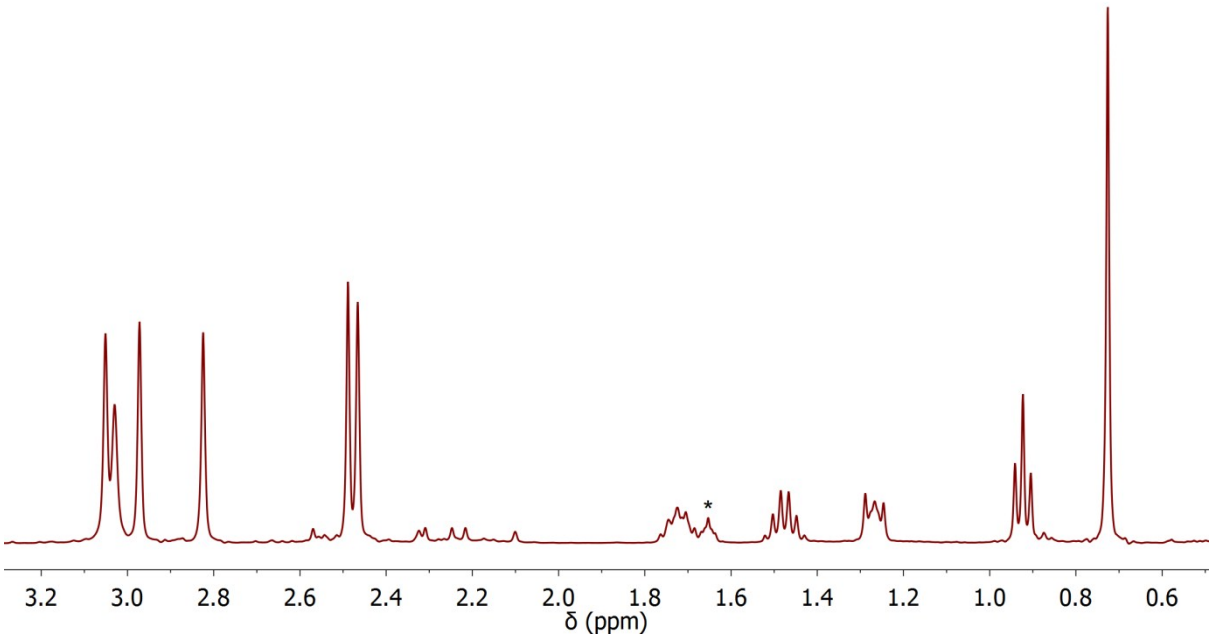

Fig. S5 ^{1}H NMR spectrum of LiInd$^{\#}$SiMe$_2$^{n}Bu in pyridine-d_5. The asterisk denotes residual thf.

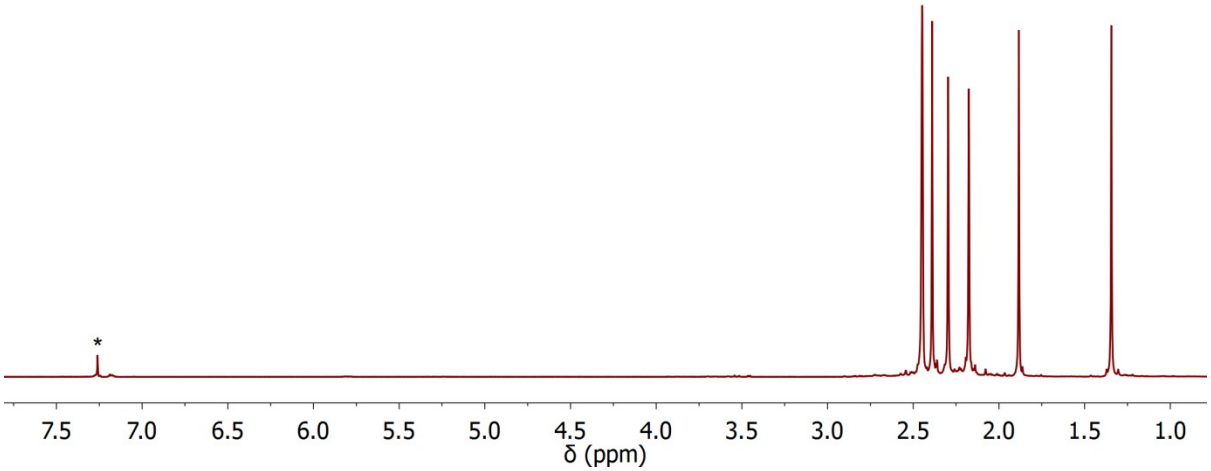

Fig. S6 ^{1}H NMR (400 MHz) spectrum of *rac*-(SBI*)$ZrCl_2$ in chloroform-d_1. Asterisk marks the residual *protio*-solvent resonance.

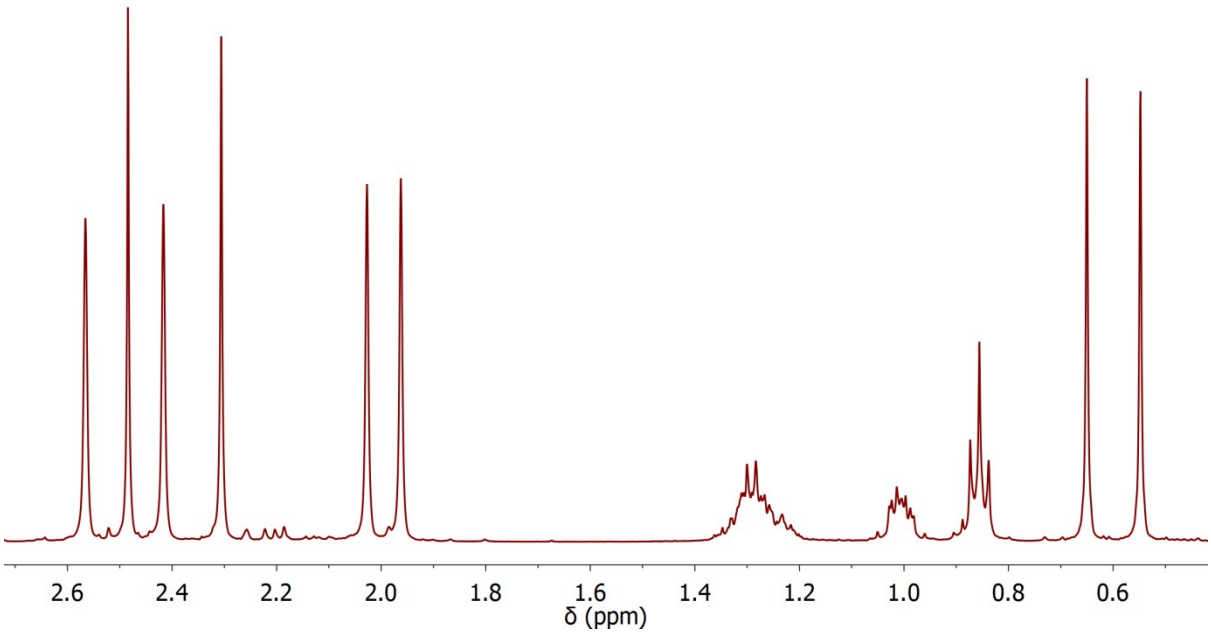

Fig. S7: ^{1}H NMR spectrum of $[(Ind^*SiMe_2{}^{n}Bu)Zr(\mu\text{-}Cl)Cl_2]_2$ in benzene-d_6.

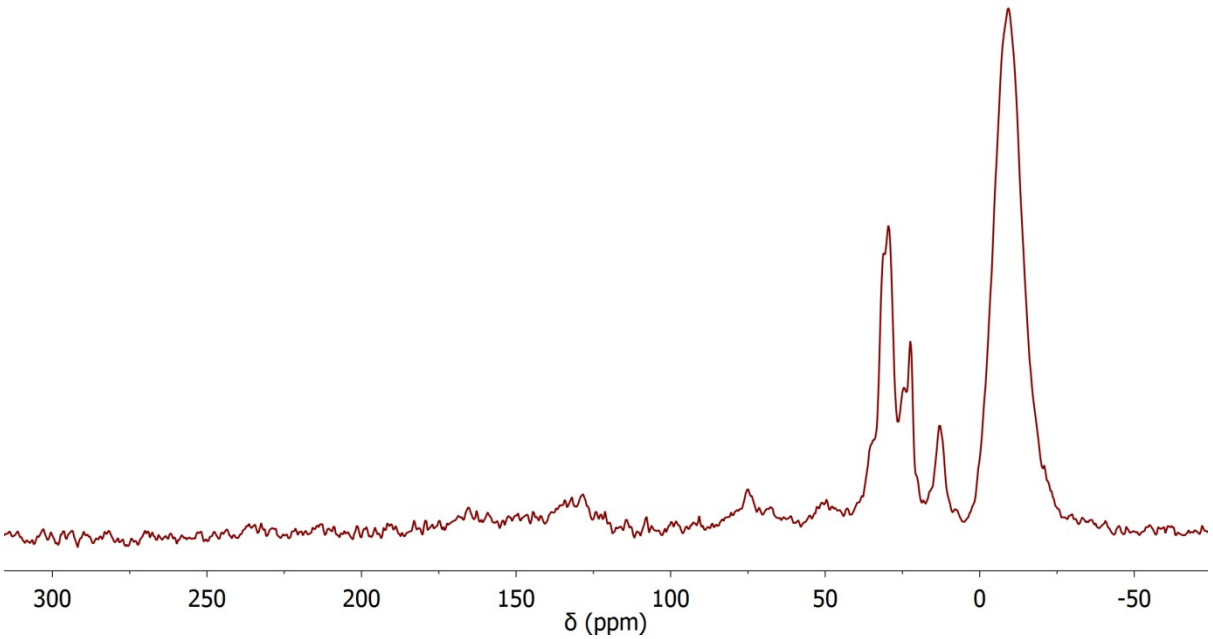

Fig. S8 ^{13}C CPMAS (10 kHz) NMR spectrum of LDHMAO-(SBI*)$ZrCl_2$.

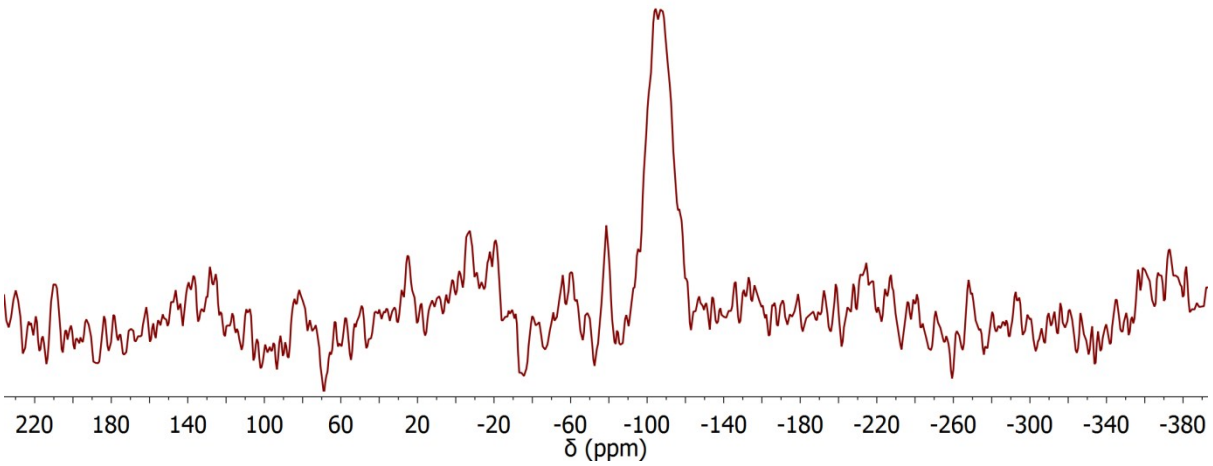

Fig. S9: ^{29}Si CPMAS (10 kHz) NMR spectrum of SSMAO-*rac*-(SBI*)$ZrCl_2$.

4. SEM

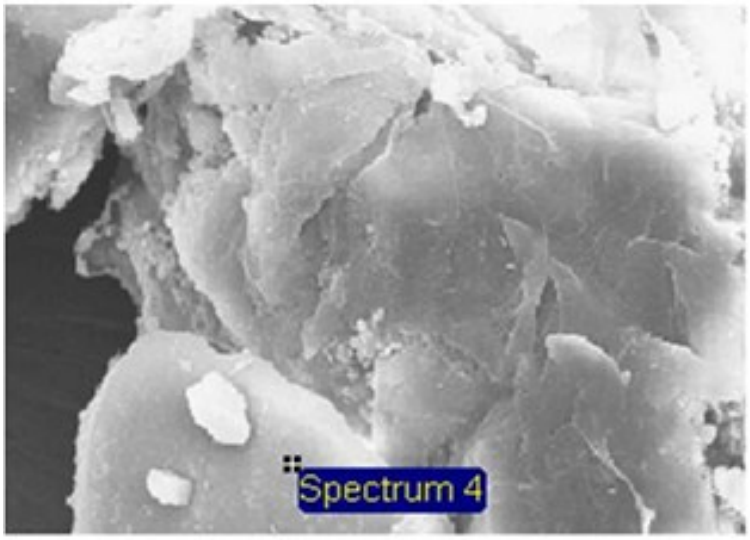

Fig. S10 SEM-EDX characterisation of SSMAO-*rac*-(EBI*)$ZrCl_2$ (SiO_2:MAO:(*rac*-EBI*)$ZrCl_2$ = 2:1:0.0050) supported on silica.

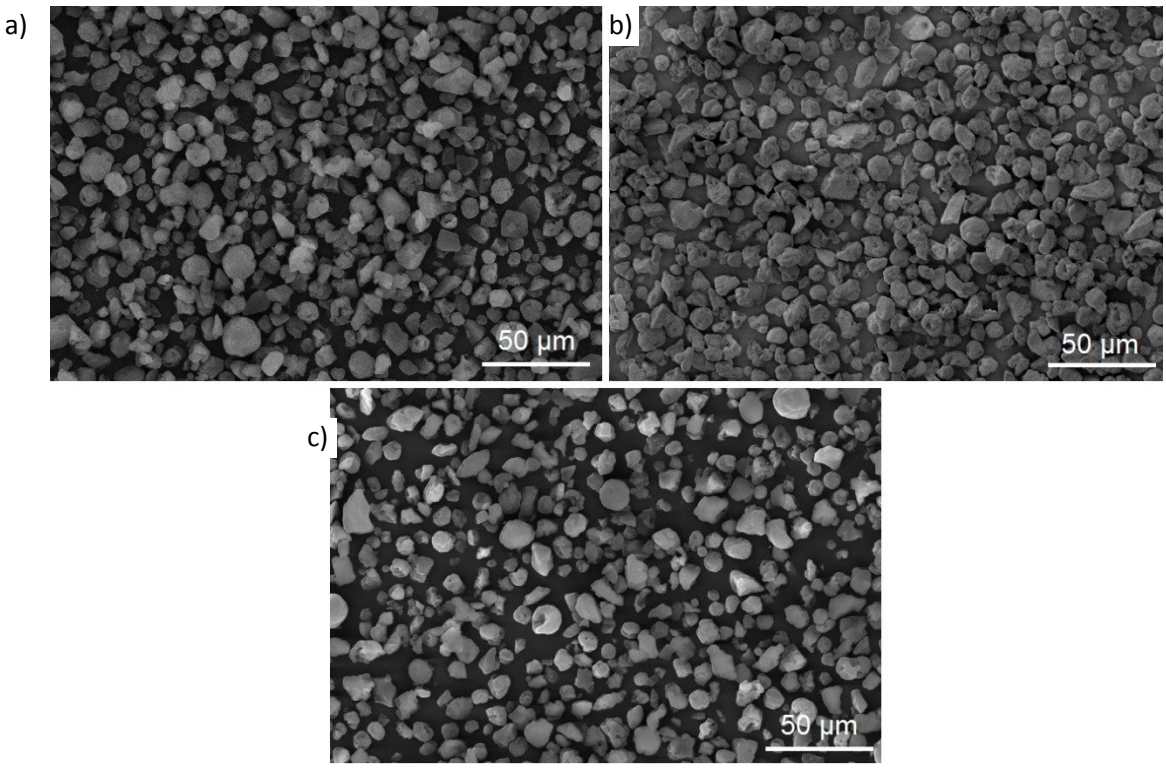

Fig. S11 Scanning electron microscopy images at 500× magnification. a) amorphous SiO_2 (Grace); b) SSMAO; c) SSMAO-(SBI*)$ZrCl_2$.

5. Definition of structural parameters

The indenyl rings will be labelled as shown in Figure S12.

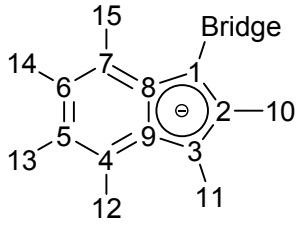

Fig. S12: Labelling scheme used in this paper.

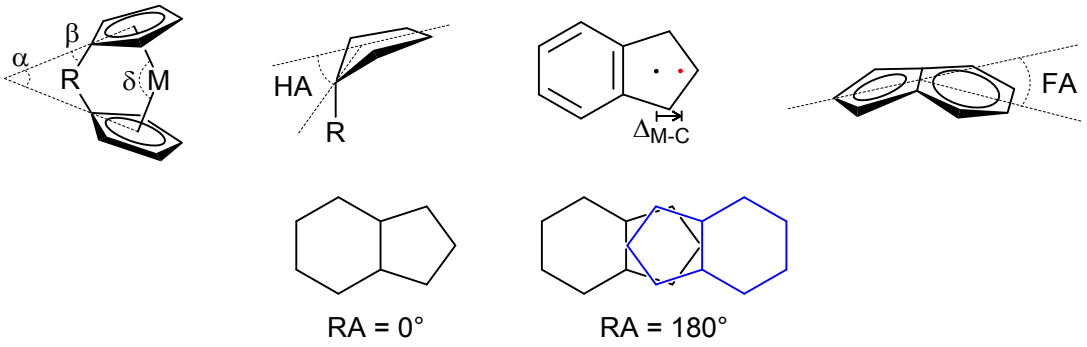

Fig. S13: Structural parameter definitions used throughout this paper.

Perhaps the most discussed parameter for group 4 metallocenes is α, a measure of the tilt between the two cyclopentadienyl rings. This parameter is measured as the dihedral angle between two planes, each calculated as the least squares mean of the five atoms comprising the Cp ring. For a perfectly tetrahedral metal centre, a value of 70.53° is expected.

A closely related angle is that of δ, which is the angle subtended at the metal centre by the normal of the two ring planes. Consequently, it is expected to be the supplementary angle to α; 109.47° for a perfect tetrahedral structure. In practice, it is measured in this work as the angle subtended at the metal centre by the two metal centroids. Any deviation between this angle (sometimes referred to elsewhere as β) and δ can indicate a degree of ring slippage; this is not expected to be significant in the d^0 metallocenes.

β, measures the angle between the first bridging atom and the plane of the Cp ring, and is used as another indicator of the strain placed on the ring by the *ansa*-bridge. While some examples display values of 30° or more, it is typically much lower than this for multi-atomic bridges. In this work, it is measured as the angle subtended at C(1) by the nearest bridging atom and the Cp_{cent}. With small values for β (<7°), its significance can largely be ignored, as the direction of the bend can be away from the metal centre.

The hinge angle (HA) can be used to describe two effects, depending on where the hinge is defined. Seen more for late transition metal indenyl chemistry, it can quantify folding in the Cp ring to accommodate a change in hapticity from η^5 to η^3 – this typically takes place at the 2-position, across the C(1)-C(3) line.

A related parameter is the fold angle (FA), which defines the dihedral angle between the planes of the benzene and cyclopentadiene rings, along the C(8)-C(9) ring annulation. This parameter can indicate

interaction with the delocalised π-system of the arene, used to stabilise electronically deficient complexes.

$\Delta_{M\text{-}C}$, also called the ring-slip parameter, is a measure of how far the metal distorts from η^5 bonding towards η^3 and is a good quantifier of the "indenyl effect". It is measured in angstroms and is calculated using Equation S1 where C(#) = M-C(#).

$$\Delta_{M-C} = \left\{\frac{C(8) + C(9)}{2}\right\} - \left\{\frac{C(1) + C(2) + C(3)}{3}\right\}$$

Equation S1: Definition of $\Delta_{M\text{-}C}$.

The rotation angle (RA), and the torsion angle (TA and TA′) all measure the twist of the two indenyl rings relative to one another with 0° being eclipsed, 180° being staggered and anything in between gauche.

6. Polymerisation data

Table S7. Solution phase ethylene polymerisation data using *rac*-(SBI*)$ZrCl_2$ – Temperature variation. Polymerisation conditions: $[MAO]/_0[Zr]_0$ = 2000, 50 mL hexanes, 2 bar.

Catalyst	Time (h)	T (°C)	Activity ($kg_{PE}/mol_{Zr}/h/bar$)	M_w (kg/mol)	M_w/M_n
rac-(SBI*)$ZrCl_2$	0.5	40	1159 ± 102	-	-
rac-(SBI*)$ZrCl_2$	0.5	50	1124 ± 174	-	-
rac-(SBI*)$ZrCl_2$	0.083	60	22622 ± 10398	213927	2.32
rac-(SBI*)$ZrCl_2$	0.067	70	18703 ± 1268	261337	2.47
rac-(SBI*)$ZrCl_2$	0.167	80	8130 ± 384	199083	2.74
rac-(SBI*)$ZrCl_2$	0.167	90	5690 ± 360	-	-

Table S8. Solution phase ethylene polymerisation data using *rac*-(SBI*)$ZrCl_2$ – scavenger amount and type variation. Polymerisation conditions: 70 °C, 50 mL hexanes, 2 bar.

Catalyst	Time (h)	$[Al]_0/[Zr]_0$	Al	Activity ($kg_{PE}/mol_{Zr}/h/bar$)	M_w (kg/mol)	M_w/M_n
rac-(SBI*)$ZrCl_2$	0.2	200	MAO	3996 ± 720	204374	2.43
rac-(SBI*)$ZrCl_2$	0.167	500	MAO	5486 ± 320	271713	2.54
rac-(SBI*)$ZrCl_2$	0.1	1000	MAO	11562 ± 1953	274106	2.51
rac-(SBI*)$ZrCl_2$	0.067	2000	MAO	18703 ± 1268	261337	2.47
rac-(SBI*)$ZrCl_2$	0.5	2000	TIBA	3 ± 2	-	-
rac-(SBI*)$ZrCl_2$	0.5	2000	TMA	0	-	-

Table S9. Slurry phase ethylene polymerisation data using SSMAO/ *rac*-(EBI*)$ZrCl_2$ – Temperature and time variation. Polymerisation conditions: $[TIBA]_0/[Zr]_0$ = 2000, 50 mL hexanes, 2 bar.

Catalyst	Time (h)	T (°C)	Activity ($kg_{PE}/mol_{Zr}/h/bar$)	M_w (kg/mol)	M_w/M_n
SSMAO/ *rac*-(EBI*)$ZrCl_2$	1	50	1650 ± 152	201417	3.02
SSMAO/ *rac*-(EBI*)$ZrCl_2$	1	60	2151 ± 12	202746	2.98
SSMAO/ *rac*-(EBI*)$ZrCl_2$	1	70	1939 ± 60	213927	3.13
SSMAO/ *rac*-(EBI*)$ZrCl_2$	1	80	1578 ± 81	198964	3.42
SSMAO/ *rac*-(EBI*)$ZrCl_2$	1	90	777 ± 16	162273	2.15
SSMAO/ *rac*-(EBI*)$ZrCl_2$	0.25	70	3012 ± 160	203759	2.54
SSMAO/ *rac*-(EBI*)$ZrCl_2$	0.5	70	2647 ± 109	196093	2.44
SSMAO/ *rac*-(EBI*)$ZrCl_2$	2	70	1414 ± 64	204610	1.94

Table S10. Slurry phase ethylene polymerisation data using SSMAO/ *rac*-(EBI*)$ZrCl_2$ – Temperature and time variation. Polymerisation conditions: $[TIBA]_0/[Zr]_0$ = 2000, 50 mL hexanes, 2 bar.

Catalyst	Time (h)	T (°C)	Activity ($kg_{PE}/mol_{Zr}/h/bar$)	M_w (kg/mol)	M_w/M_n
SSMAO/ *rac*-(SBI*)$ZrCl_2$	0.5	40	354 ± 70	261002	2.96
SSMAO/ *rac*-(SBI*)$ZrCl_2$	0.5	50	591 ± 12	245928	3.05
SSMAO/ *rac*-(SBI*)$ZrCl_2$	0.5	60	651 ± 28	258536	3.00
SSMAO/ *rac*-(SBI*)$ZrCl_2$	0.5	70	611 ± 10	261956	3.21
SSMAO/ *rac*-(SBI*)$ZrCl_2$	0.5	80	759 ± 24	197594	2.69
SSMAO/ *rac*-(SBI*)$ZrCl_2$	0.5	90	637 ± 20	160049	2.56

SSMAO/ *rac*-(SBI*)$ZrCl_2$	0.25	70	709 ± 21	226299	2.79
SSMAO/ *rac*-(SBI*)$ZrCl_2$	1	70	625 ± 31	242928	2.96
SSMAO/ *rac*-(SBI*)$ZrCl_2$	2	70	497 ± 47	183865	2.64

Table S11. Slurry phase ethylene polymerisation data using LDHMAO/ complex – Catalyst variation. Polymerisation conditions: $[TIBA]_0/[Zr]_0$ = 2000, 1 h, 70 °C, 50 mL hexanes, 2 bar.

Catalyst	Activity ($kg_{PE}/mol_{Zr}/h/bar$)	M_w (kg/mol)	M_w/M_n
(MgAl-SO_4)-LDHMAO/ *rac*-(EBI)$ZrCl_2$	1841	194134	4.08
(MgAl-SO_4)-LDHMAO/ *rac*-(EBI*)$ZrCl_2$	4325	251512	2.36
(MgAl-SO_4)-LDHMAO/ *rac*-(SBI*)$ZrCl_2$	9657	276905	2.40
(MgAl-Cl)-LDHMAO/ *rac*-(EBI*)$ZrCl_2$	2374	264690	2.21
(MgAl-CO_3)-LDHMAO/ *rac*-(EBI*)$ZrCl_2$	2720	293530	2.06

7. References

(1) Cosier, J.; Glazer, A. M. *J. Appl. Crystallogr.* **1986**, *19*, 105.
(2) Otwinowski, Z.; Minor, W. *Methods Enzymol.* **1997**, *276*, 307.
(3) Blessing, R. H. *Acta Crystallogr. Sect. A* **1995**, *51*, 33.
(4) CrysAlisPRO, Oxford Diffraction/Agilent Technologies UK Ltd, Yarnton, England.
(5) G. M. Sheldrick, Acta Crystallogr., Sect. A: Found. Crystallogr., 2008, 64, 112-122.
(6) Palatinus, L.; Chapuis, G. *J. Appl. Crystallogr.* **2007**, *40*, 786.
(7) Betteridge, P. W.; Carruthers, J. R.; Cooper, R. I.; Prout, K.; Watkin, D. J. *J. Appl. Crystallogr.* **2003**, *36*, 1487.
(8) Cooper, R. I.; Thompson, A. L.; Watkin, D. J. *J. Appl. Crystallogr.* **2010**, *43*, 1100.
(9) L. J. Farrugia, J. Appl. Crystallogr., 1999, 32, 837-838.
(10) Macrae, C. F.; Bruno, I. J.; Chisholm, J. A.; Edgington, P. R.; McCabe, P.; Pidcock, E.; Rodriguez-Monge, L.; Taylor, R.; Van De Streek, J.; Wood, P. A. *J. Appl. Crystallogr.* **2008**, *41*, 466.
(11) Spek, A. L. *J. Appl. Crystallogr.* **2003**, *36*, 7.
(12) M. N. Burnett and C. K. Johnson, ORTEP-III Report ORNL-6895. Oak Ridge National Laboratory, Tennessee, USA, 1996.

(13) F. Neese, Orca − an ab initio, DFT and Semiempirical Electronic Structure Package, Version2.8, Revision 2360; Institut für Physikalische und Theoretische Chemie, Universität Bonn, Bonn (Germany)).
(14) A. D. Becke, *J. Chem. Phys.*, 1986, **84**, 4524.
(15) J. P. Perdew and W. Yue, *Phys. Rev. B: Condens. Matter Mater. Phys.*, 1986, **33**, 8800.
(16) J. P. Perdew, *Phys. Rev. B: Condens. Matter Mater. Phys.*, 1986, **33**, 8822.
(17) C. Lee, W. Yang and R. G. Parr, *Phys. Rev. B: Condens. Matter Mater. Phys.*, 1988, **37**, 785.
(18) A. D. Becke, *J. Chem. Phys.*, 1993, **98**, 5648.
(19) D. A. Pantazis, X.-Y. Chen, C. R. Landis and F. Neese, *J. Chem. Theory Comput.*, 2008, **4**, 908.
(20) D. A. Pantazis and F. Neese, *J. Chem. Theory Comput.*, 2009, **5**, 2229.
(21) A. Schäfer, C. Huber and R. Ahlrichs, *J. Chem. Phys.*, 1994, **100**, 5829.
(22) F. Weigend and R. Ahlrichs, *PCCP*, 2005, **7**, 3297.
(23) F. Weigend, *PCCP*, 2006, **8**, 1057.
(24) K. Eichkorn, F. Weigend, O. Treutler and R. Ahlrichs, *Theor. Chem. Acc.*, 1997, **97**, 119.
(25) K. Eichkorn, O. Treutler, H. Öhm, M. Häser and R. Ahlrichs, *Chem. Phys. Lett.*, 1995, **242**, 652.
(26) K. Eichkorn, O. Treutler, H. Öhm, M. Häser and R. Ahlrichs, *Chem. Phys. Lett.*, 1995, **240**, 283.
(27) E. F. Pettersen, T. D. Goddard, C. C. Huang, G. S. Couch, D. M. Greenblatt, E. C. Meng and T. E. Ferrin, *J. Comput. Chem.*, 2004, **25**, 1605.